Dalton Transactions

ROYAL SOCIETY OF CHEMISTRY

PAPER

View Article Online
View Journal | View Issue

Cite this: *Dalton Trans.*, 2021, **50**, 5154

The mechanism of the gold(I)-catalyzed Meyer–Schuster rearrangement of 1-phenyl-2-propyn-1-ol *via* 4-*endo*-*dig* cyclization†

Diego Sorbelli, [a] Jacopo Segato,[b] Alessandro Del Zotto, [b] Leonardo Belpassi, [c] Daniele Zuccaccia *[b] and Paola Belanzoni *[a,c]

Received 9th January 2021,
Accepted 25th February 2021

DOI: 10.1039/d1dt00080b

rsc.li/dalton

With the aim of rationalizing the experimental counterion- and solvent-dependent reactivity in the gold (I)-catalyzed Meyer–Schuster rearrangement of 1-phenyl-2-propyn-1-ol, a computational mechanistic study unraveled the unexpected formation of a gold-oxetene intermediate *via* commonly unfavorable 4-*endo*-*dig* cyclization triggered by the counterion in low polarity solvents.

Introduction

Gold-catalyzed transformations of propargyl alcohols have become very popular since these species possess both a nucleophilic hydroxy group and a potentially electrophilic alkyne moiety, and gold, as a soft Lewis acid, can efficiently activate them. To date, several gold-catalyzed chemical transformations of these substrates have been reported.[1] Among others, the Meyer–Schuster (MS) rearrangement is one of the most popular reactions, since it can deliver α,β-unsaturated carbonyl compounds with complete atom economy.[2] Gold catalysts allow one to carry out this rearrangement with high yields under mild experimental conditions.[1] Despite all the experimental advances in the gold-catalyzed MS rearrangement, unfortunately a deep and complete understanding of the catalytic mechanism is still lacking. Throughout the years, a variety of mechanisms have been proposed on the basis of experimental results.[3] As an example, a mechanistic study on the NHC-gold(I)-catalyzed (NHC = N-heterocyclic carbene) MS rearrangement of propargylic acetates suggested an unusual gold-hydroxy complex as the active catalytic species.[4]

All the proposed mechanisms share two common features. Firstly, the role of the counterion is completely neglected in the calculations, although the counterion effect has been shown to be crucial for understanding the reactivity in similar gold catalyzed processes.[5–8] Secondly, the reported mechanisms only take into account the presence of either water or alcohols as solvents, thus not accounting for the use of other organic and green solvents. The replacement of volatile organic solvents (VOS) with green solvents or performing the reaction under neat conditions is a key topic in organic synthesis, but it is rare in gold catalysis.[9]

In this work, experimental evidence for both solvent and counterion effects is given for the MS rearrangement of 1-phenyl-2-propyn-1-ol to cinnamaldehyde at 50 °C catalyzed by NHC-Au-X (**1-X**: NHC = 1,3-bis(2,6-di-isopropylphenyl)-imidazol-2-ylidene; X^- = Cl^-, BF_4^-, OTf^-, OTs^-, and TFA^-) (Scheme 1; for further details, see Fig. S1, S2 and Tables S1, S2 in the ESI†). Here, VOS and green solvents, with different polarity and functional groups, have been analysed.

Density functional theory (DFT) and *ab initio* calculations have been performed to study the reaction mechanism, which allowed us to rationalize the experimental results and clarify the counterion- and solvent-dependent reactivity. This study provides new insights not only into the MS mechanism but also into the experimental conditions that may modify it and it should be helpful in the design of new MS rearrangement reactions. Remarkably, this work further consolidates the use of green solvents instead of traditional VOS.

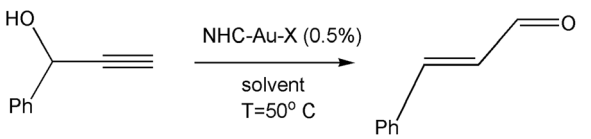

Scheme 1 Schematic representation of the experimentally studied reaction.

[a]*Department of Chemistry, Biology and Biotechnology, University of Perugia, Via Elce di Sotto 8, I-06123 Perugia, Italy. E-mail: paola.belanzoni@unipg.it*
[b]*Dipartimento di Scienze Agroalimentari, Ambientali e Animali, Sezione di Chimica, Università di Udine, Via Cotonificio 108, I-33100 Udine, Italy. E-mail: daniele.zuccaccia@uniud.it*
[c]*Institute of Chemical Sciences and Technologies "Giulio Natta" of CNR (CNR-SCITEC), c/o Department of Chemistry, Biology and Biotechnology, University of Perugia, Via Elce di Sotto 8, I-06123 Perugia, Italy*
†Electronic supplementary information (ESI) available. See DOI: 10.1039/d1dt00080b

Results and discussion

In Fig. 1 and Table 1, the experimental results involving the gold-catalyzed Meyer–Schuster rearrangement of 1-phenyl-2-propyn-1-ol are shown (for experimental procedure details, see the ESI, Tables S1, S2 and Fig. S1, S2†). Complex **1**-OTf was inefficient in DMSO, as no formation of the product was observed after 24 h (Table 1, entry 17). This can be related to its remarkable coordination ability towards gold.[9] In contrast, high or even quantitative formation of cinnamaldehyde was achieved within 1–24 h using other solvents or under neat conditions (Table 1 and Fig. 1).

In the case of VOS, a high conversion of 1-phenyl-2-propyn-1-ol into cinnamaldehyde was achieved in 0.5 h in chloroform (Table 1, entry 1) without the formation of other side products. Much less efficiently, **1**-OTf promoted the formation of the reaction product in rather low yield (12–13% after 0.5 h) in dichloromethane and acetone (Table 1, entries 2 and 3, respectively; Fig. 1).

High conversions were generally attained using neoteric solvents (Table 1 and Fig. 1). A high conversion was achieved after 0.5 h using low-polarity solvents such as *p*-cymene, limonene, and anisole (Table 1, entries 4, 12 and 13, respectively), while about a half conversion was achieved using ethyl lactate, furfuryl alcohol and γ-valerolactone (Table 1, entries 14, 15 and 16, respectively). The reaction proceeded slowly in methyl levulinate (Table 1, entry 18).

In order to study the importance of the counterion, the catalysis was conducted in *p*-cymene with **1**-Cl/AgX (X = BF_4^-, OTf^-, OTs^-, and TFA^-) as the catalytic system. It was found that the efficiency strongly depends on the counterion: conversions of 30%, 11%, 7% and 0.4% were observed after 30 min for OTf^-, OTs^-, BF_4^-, and TFA^-, respectively (Table 1, entries 5–8).

On comparing the conversion achieved by **1**-OTf (Table 1, entry 4) with that shown by the *in situ* generated complex (**1**-Cl + AgOTf) (Table 1, entry 8), a neat decrease was observed in the latter case. This may suggest a negative effect of the silver ion,[10] but the presence of induction time related to the activation of the catalyst cannot be excluded.

A deep comparison of the catalytic activity of the gold catalyst in different solvents was made by examining the TOF value [TOF (h^{-1}) = moles of the product per moles of the catalyst per

Table 1 **1**-X catalyzed Meyer–Schuster rearrangement of 1-phenyl-2-propyn-1-ol to cinnamaldehyde at 50 °C[a]

Entry	Solvent	Catalytic system[b]	Conv.[b] %	TOF[c] (h^{-1})	ε_r[d]
VOS					
1	Chloroform	**1**-OTf	75	300	4.81
2	Dichloromethane	**1**-OTf	12	53	8.93
3	Acetone	**1**-OTf	13	50	21
Green					
4	*p*-Cymene	**1**-OTf	91	394	2.24
5	*p*-Cymene[e]	**1**-Cl/AgOTs	11	44	2.24
6	*p*-Cymene[f]	**1**-Cl/AgTFA	0.4	2	2.24
7	*p*-Cymene[g]	**1**-Cl/$AgBF_4$	7	28	2.24
8	*p*-Cymene[h]	**1**-Cl/AgOTf	30	115	2.24
9	*p*-Cymene[i]	**1**-OTf/HOTf	100	400	2.24
10	*p*-Cymene[j]	**1**-OTf/HOTs	93	371	2.24
11	*p*-Cymene[k]	**1**-OTf/PS	0	0	2.24
12	Limonene	**1**-OTf	67	246	2.4
13	Anisole	**1**-OTf	85	368	4.3
14	Ethyl lactate	**1**-OTf	24	106	15.4
15	Furfuryl alcohol	**1**-OTf	37	161	16.9
16	γ-Valerolactone	**1**-OTf	23	105	36.9
17	DMSO	**1**-OTf	0	0	46.7
18	Methyl levulinate	**1**-OTf	17	74	—
19	—[l]	**1**-OTf	74	296	—

[a] Catalysis conditions: NHC-Au-OTf (0.0025 mmol, 1.8 mg), 1-phenyl-2-propyn-1-ol (0.5 mmol, 61 μL), solvent (200 μL). [b] Determined by ^{1}H NMR; the average value of three measurements after 30 minutes. [c] TOF = ($mol_{product}/mol_{catalyst}$)/$t$ calculated after 30 minutes. [d] ε_r = dielectric constant. [e] NHC-Au-Cl (0.0025 mmol, 1.6 mg), 1.1 eq. AgOTs. [f] NHC-Au-Cl (0.0025 mmol, 1.6 mg), 1.1 eq. AgTFA. [g] NHC-Au-Cl (0.0025 mmol, 1.6 mg), 1.1 eq. $AgBF_4$. [h] NHC-Au-Cl (0.0025 mmol, 1.6 mg), 1.1 eq. AgOTf. [i] NHC-Au-OTf (0.0025 mmol, 1.8 mg), 10% (with respect to the substrate) HOTf. [j] NHC-Au-OTf (0.0025 mmol, 1.8 mg), 10% (with respect to the substrate) HOTs. [k] NHC-Au-OTf (0.0025 mmol, 1.8 mg), 10% (with respect to the substrate) proton sponge (1,8-bis(dimethylamino)naphthalene). [l] No solvent was used.

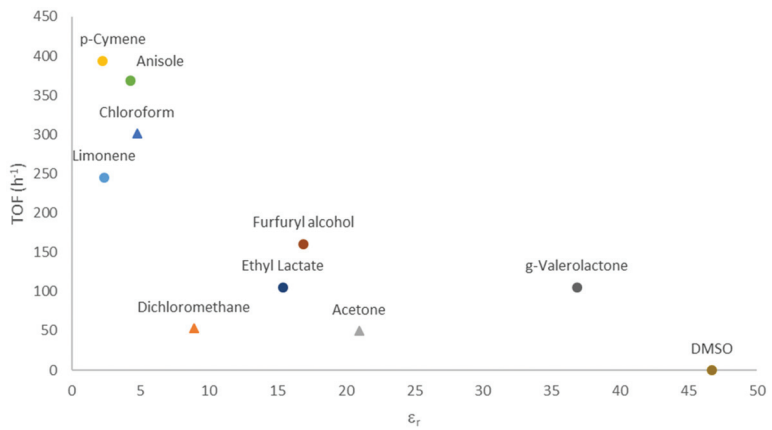

Fig. 1 TOF *vs.* dielectric constant for the **1**-OTf catalyzed Meyer–Schuster rearrangement of 1-phenyl-2-propyn-1-ol to cinnamaldehyde at 50 °C (selected values from Table 1).

time] (Table 1). The calculated TOF values span from 0 h^{-1} (DMSO) to 394 h^{-1} (*p*-cymene) (Table 1, entries 17–4). A general trend can be observed: the TOF value decreases when the polarity of the solvent increases (Table 1 and Fig. 1); this is also observed in the gold catalyzed methoxylation of 3-hexyne.[9]

In addition, in *p*-cymene the catalytic efficiency strongly depends on the counterion, according to the following order: OTf^- > OTs^- > BF_4^- > TFA^- (Table 1, compare entries 4–7). This finding, combined with the observed trend of TOF *vs.* ε_r, suggests the role of the anion during the reaction. Compared to the related study in ref. 4, in which the presence or absence of water in the reaction mixture was found to be crucial, here the observed trend of TOF in different solvents and the activity of **1**-X in *p*-cymene suggest that the role of water under our catalytic conditions is much less important with respect to the role of the anion.

We also investigated the effect of the addition of Brønsted acids and bases. The addition of HOTf and HOTs does not alter the reaction rate and the TOF values remain around 371–400 h^{-1} (compare entries 4, 9, and 10 in Table 1), also indicating that, under acidic conditions, the rate does not depend on the counterion. On the other hand, the catalysis is completely inhibited when the proton sponge (PS) 1,8-bis(dimethylamino)naphthalene (Table 1, entry 11) is added to the catalytic mixture. A possible explanation can be found in the formation of a stable σ-bonded gold-alkynyl complex through the abstraction of the acidic hydrogen atom of the terminal alkyne by PS (see below).

Finally, an intermediate catalytic performance is observed when the reaction is performed in γ-valerolactone (GVL), a commonly employed green solvent,[11] despite its high dielectric constant, and also when the reaction is performed under neat conditions (Table 1, entries 16 and 19), thus indicating that a green version of the reaction is feasible.

Based on these experimental results and motivated by the lack of a general mechanistic comprehension,[12] a computational study has been carried out to both rationalize the experimental outcome and gain further insights into the yet elusive mechanism of the gold-catalyzed MS rearrangement. A commonly accepted mechanism for gold(I)-catalyzed reactions with alkyne substrates consists of: (i) a pre-equilibrium step, in which the gold-coordinated anion is replaced with the alkyne; (ii) a nucleophilic attack step, in which the activated alkyne is attacked by a nucleophile, with the formation of an organogold intermediate; and (iii) a protodeauration step, in which the gold–carbon bond in the intermediate is typically cleaved by a proton to give the product and regenerate the catalyst. A pivotal counterion effect has been previously found by some of us in each step of this reaction mechanism.[7]

With the aim of explaining the counterion-dependent reactivity observed in this MS rearrangement, the gold-catalyzed intramolecular nucleophilic attack is considered in our study, where a model [NHC′-Au-X] (NHC′ = 1,3-dimethylimidazol-2-ylidene; X^- = OTf^-, OTs^-, and BF_4^-) complex is used. This step has been previously found to be the rate-determining step

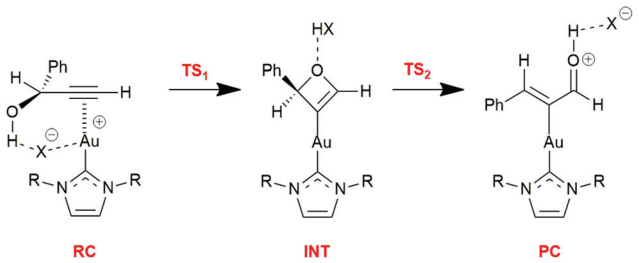

Scheme 2 DFT mechanism of the intramolecular nucleophilic attack in the 1-phenyl-2-propyn-1-ol rearrangement catalyzed by the $[Au\text{-}NHC']^+$ complex and assisted by three different counterions (X^- = OTf^-, OTs^- and BF_4^-).

(RDS) in similar reactions.[9] The schematic representation of the resulting mechanism is shown in Scheme 2. The geometries of the stationary points and transition states have been optimized at the DFT level including both dispersion and relativistic effects (BP86/ZORA/D3). Single-point energy calculations have been performed at both DFT (B2PLYP/CPCM) and DLPNO-CCSD(T)[13] levels (see the ESI† for computational details). All the optimized geometries are shown in Fig. S3–S5 in the ESI.†

Based on the well-known ability of gold to activate triple bonds, we started our investigation by considering the cationic $[Au\text{-}NHC']^+$ fragment coordinated to the alkyne moiety as our reactant complex (RC). In principle, we expect the RC to directly convert into the product complex (PC), *i.e.*, a gold-aldehyde species, that should yield cinnamaldehyde and regenerate the catalyst through protodeauration. Surprisingly, we find that, independently of the nature of the counterion, a gold-oxetene intermediate (INT) is formed *via* 4-*endo-dig* cyclization, and it subsequently undergoes electrocyclic ring opening and yields the expected PC (Scheme 2). The mechanism we propose here is able to rationalize the observed reactivity. As depicted in Scheme 2, the counterion in this reaction plays a key role, since it behaves as a hydrogen-bond acceptor, by increasing the nucleophilicity of the attacking hydroxy group, and as a template, helping the hydroxy group to assume its reactive position through simultaneous interaction with the OH hydrogen and the gold center. Furthermore, it acts as a "proton shuttle", by transferring the proton from the intermediate to generate the PC. Clearly, the different basicity nature and coordination ability of the counterions result in a very different reactivity, with the reaction yields and TOF values highly depending on it (Table 1). In particular, the anion is known to act as a catalyst deactivator, by its either strong coordinating or basicity power, in the pre-equilibrium step of the reaction.[7] Preliminary calculations have been performed for this step by comparing the strongest coordinating/basic OTf^-, OTs^- and TFA^- anions, which have allowed us to immediately rationalize the poorest efficiency of TFA^-. The results (Fig. S6 in the ESI†) show that whereas the expected gold-alkyne complex is obtained for OTf^- and OTs^-, a stable σ-bonded gold-alkynyl complex is formed through the abstrac-

tion of the acidic hydrogen atom of the terminal alkyne by TFA^- with a low energy barrier (5.0 kcal mol^{-1}); see the experimental part below. The formation of such a complex, due to the strongest basicity of TFA^- in the anion series and its bidentate nature, prevents the π activation of the triple bond and is consistent with the experimentally observed lowest efficiency of TFA^-. Therefore, only OTf^-, OTs^- and BF_4^- anions have been compared in the nucleophilic attack step, starting from a suitable RC conformation, where the anion occupies a bridging position between the gold center and the attacking OH group. The calculated energy profiles highlight the substantial differences, as shown in Fig. 2.

In Fig. 2, we observe that, for the OTf^--assisted intramolecular attack, the lowest activation barrier is obtained (32.6 kcal mol^{-1}), whereas when the OTs^- and BF_4^- anions are involved, the barriers are higher (34.3 and 36.9 kcal mol^{-1}, respectively), which is in full agreement with the experimentally observed reactivity trend. Note that, somewhat arbitrarily, we use the reactant complex RC as the zero energy reference point. On the other hand, by taking the sum of the energy of the isolated reactant and catalyst as the zero energy reference point, we get a much lower value of the energy barrier (for instance, 24.3 and 20.7 kcal mol^{-1} for OTs^- and OTf^-, respectively). This is because in a low polarity solvent, like *p*-cymene, we deal with almost 100% ion pairing between the $[NHC'\text{-}Au]^+$ catalyst and X-counterion, which is very likely. Under these experimental conditions, the isolated reactants are represented by neutral [NHC′-Au-X] and 1-phenyl-2-propyn-1-ol species, whose energy is higher than that of the RC, where stabilizing interactions between the reactants, such as hydrogen bonds, take place. For this reason, we use the RC energy as the zero energy reference point, still obtaining an activation barrier trend that nicely reproduces the experimental counterion-dependent reactivity.

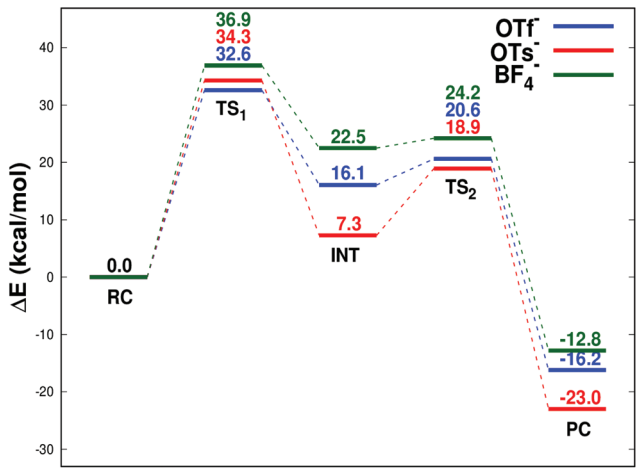

Fig. 2 Energy profiles (BP86/ZORA/D3//B2PLYP/CPCM; see the ESI† for details) for the intramolecular nucleophilic attack in the 1-phenyl-2-propyn-1-ol rearrangement catalyzed by the $[Au(I)\text{-}NHC']^+$ complex and assisted by three different counterions (X^- = OTf^-, in blue; OTs^-, in red; and BF_4^-, in green). Energy values refer to the corresponding reactant complex RC taken as zero.

The enthalpy and Gibbs free energy profiles computed at the BP86/ZORA/D3//BP86/ZORA/D3 level are also presented in Fig. S7–S9 in the ESI,† showing that electronic energy $\Delta E^{\#}$ can be considered as a good approximation to $\Delta G^{\#}$. The reaction profiles calculated using different computational setups (BP86/ZORA//B2PLYP, BP86/ZORA/D3//B2PLYP and BP86/ZORA/D3//DLPNO-CCSD(T)) are compared in Fig. S10–S12 in the ESI,† showing that they are quantitatively similar. Finally, we also examined the solvation effect on the geometries of the stationary points by performing optimization calculations including the solvent with the COSMO model. As shown in Fig. S13 and S14 in the ESI,† the reaction profiles (X = OTf^-, OTs^-) calculated with the BP86/ZORA/D3/COSMO//B2PLYP/CPCM protocol are quantitatively very similar to those shown in Fig. 2, with the energies differing by less than 1 kcal mol^{-1}. Interestingly, the results of these test calculations fully validate the accuracy of a computational protocol based on the BP86 optimization geometry and B2PLYP single point energy calculations suggested by us for similar gold-catalyzed reactions.[14] Finally, they demonstrate the importance of solvent (*p*-cymene) inclusion to appropriately match the experimental trend, since in the gas phase almost identical barriers are calculated for OTs^- and OTf^- (31.5 *vs.* 31.6 kcal mol^{-1} at the BP86/ZORA/D3//B2PLYP level, and 32.2 *vs.* 32.6 kcal mol^{-1} at the BP86/ZORA/D3//DLPNO-CCSD(T) level, respectively). Note that the calculation of the energy barriers ($\Delta H^{\#}$) for the energy profiles in Fig. 2 by including both dispersion and solvation effects on the geometry optimizations (at the BP86/ZORA/D3/COSMO//BP86/ZORA/D3/COSMO level, Fig. S15 in the ESI†) gives 28.9, 31.4 and 32.1 kcal mol^{-1} values ($\Delta G^{\#}$ = 27.6, 30.6 and 33.7 kcal mol^{-1}) for OTf^-, OTs^- and BF_4^-, respectively, which nicely compare with the activation barrier value calculated in ref. 4 for the formation of enones *via* the Meyer–Schuster rearrangement ($\Delta H^{\#}$ = 25.4 kcal mol^{-1}), occurring in water and catalyzed by a gold-hydroxide species. Later, in this section, we also analyze this reaction path in detail. Remarkably, all the calculated reaction energy profiles (Fig. S7–S14†) are qualitatively similar to those depicted in Fig. 2. A rationalization for OTf^- favoring the intramolecular nucleophilic attack can be achieved by analyzing the three TS1 structures that are depicted in Fig. 3.

In all the TS1 structures, the anion features a bridging position between the OH group and the Au center. By comparing the hydroxy O–H distances (Fig. S3–S5 in the ESI†), we note that they match the hydrogen-bond acceptor ability of the three anions (1.021 for OTs^-, 1.016 for OTf^- and 1.001 Å for BF_4^-) but they do not correlate with the activation energy barrier trend. Based on the anion basicity strength, the best nucleophile activator OTs^- should give the lowest barrier. Instead, the X–Au distances in the RC structures (2.847 for X = OTs^-; 2.955 for X = OTf^-; 2.976 Å for X = BF_4^-) are consistent with the anion coordinating ability trend (OTs^- > OTf^- > BF_4^-). Based on the anion coordinating strength, the best CC triple bond de-activator OTs^- should give the highest barrier.

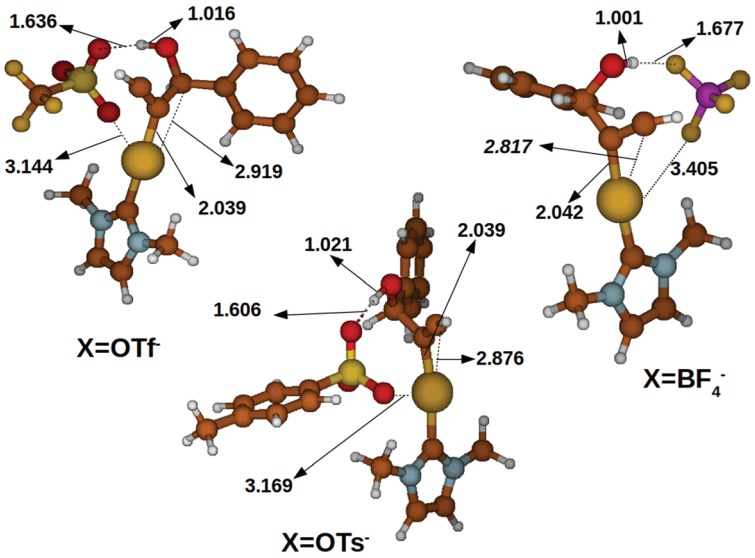

Fig. 3 Optimized structures of the TS1 transition states for the intramolecular nucleophilic attack in 1-phenyl-2-propyn-1-ol assisted by OTf^-, OTs^-, and BF_4^- counterions. The most relevant bond distances calculated at the BP86/ZORA/D3 level are shown.

However, as previously reported by some of us, the extent of alkyne slippage (*i.e.*, the $\eta^2 \rightarrow \eta^1$ deformation occurring at the alkyne coordination to gold) can be considered as a reactivity index. A larger alkyne slippage corresponds to a more electrophilic terminal carbon atom (C1) and therefore to a lower activation barrier for the nucleophilic attack.[9,15] In the TS1 structures, the Au–C1 distances (2.919 Å for X = OTf^-; 2.876 Å for X = OTs^-; 2.817 Å for X = BF_4^-) show that for the OTf^- anion-assisted attack, the largest $\eta^2 \rightarrow \eta^1$ deformation occurs, resulting in a more electrophilic C1 carbon atom and, as a consequence, resulting in the lowest activation barrier. These findings suggest that the activation of the nucleophilic hydroxy group should be counteracted by the de-activation of the electrophilic character of the CC triple bond through interaction with the gold center. Thus, the activation energy barrier appears to arise as a balance between the anion hydrogen-acceptor ability and the anion affinity towards gold (extent of alkyne slippage), which is ultimately responsible for the observed (and calculated) catalytic efficiency trend.

As mentioned above, in ref. 4, a mechanism for the gold-catalyzed formation of enones *via* the Meyer–Schuster rearrangement has been proposed in which a gold-hydroxide complex (NHC-Au-OH), generated *in situ*, is the catalytic species. It must be pointed out, however, that in the reported mechanism, water (which was used as the solvent) plays a fundamental role in the formation of the catalytically active gold-hydroxide species and in the reaction path. Under our experimental conditions, as already mentioned, such a crucial role of water in the reaction mechanism is far less conceivable, since in the *p*-cymene solvent we observe a very different catalytic efficiency when different counterions are employed, thus indicating that the role of water (even in traces) is much less important than the role of the anion in the reaction mechanism.

Nonetheless, we decided to investigate whether the mechanism proposed in ref. 4 could be feasible for the reaction studied here. The energy profile for the gold-hydroxide-catalyzed reaction is shown in Fig. S16 in the ESI† and, notably, the calculated barrier (32.1 kcal mol^{-1}) for the nucleophilic attack is very close to that obtained for the formation of the gold-oxetene intermediate (32.6 kcal mol^{-1}). In addition, we compared the thermodynamics of the gold-hydroxide species formation with that of the gold-alkyne species (RC) formation. The calculations indicate that although the two reactions are both exothermic, the gold-alkyne species is more stable than the gold-hydroxide species (−11.9 and −5.1 kcal mol^{-1}, respectively) (see Fig. S17 in the ESI†), thus suggesting that the gold-alkyne species is likely to be more abundant in solution and supporting the mechanism we propose here under our experimental conditions. The formation of a gold–water complex ($[NHC\text{-}Au\text{-}OH_2]^+$) as a possible gold species present in the reaction mixture has also been considered, and has been found to be slightly more favored (−6.1 kcal mol^{-1}) with respect to the formation of the NHC-Au-OH complex (see Fig. S17 in the ESI†). We also investigated the nucleophilic attack step in which the gold–water complex is the catalytically active species. However, the barrier for this attack (39.2 kcal mol^{-1}) is much higher than the previous ones (*i.e.*, those calculated with gold-hydroxide and gold-alkyne as the active species); thus, one can expect that the active role of the gold–water complex may be safely neglected (see Fig. S18 in the ESI†).

Finally, the preferential coordination of the gold–carbene fragment to the propargylic hydroxyl group with the formation of a gold-hydroxide species similar to that proposed as the catalytically active species in ref. 4 has also been examined. Although this species is 11.4 kcal mol^{-1} more stable than the RC, the nucleophilic attack requires a much higher activation

barrier (65.3 kcal mol^{-1}) (Fig. S19 in the ESI†) than that from the RC (31.2 kcal mol^{-1}) (at the BP86/ZORA//B2PLYP level, Fig. S10 in the ESI†). Notably, no reaction intermediate is formed in this case.

The mechanism proposed here (Scheme 2) is peculiar. We find that the 4-*endo-dig* cyclizations and the ring opening of the 4-*endo* products are feasible, although they are commonly kinetically very unfavorable.[16] To the best of our knowledge, the evidence of the gold-catalyzed synthesis of oxetenes and the presence of gold-oxetene intermediates has been reported only a few times[17] and never in the gold-catalyzed MS rearrangement.

In order to isolate and characterize the predicted gold-oxetene adduct, a stoichiometric reaction between 1-phenyl-2-propyn-1-ol and **1**-OTf in the presence of a 3-fold excess of 1,8-bis(dimethylamino)naphthalene in $CDCl_3$ was performed. Unfortunately, the abstraction of the acidic hydrogen atom of the terminal alkyne was accomplished with the formation of a stable σ-bonded gold-alkynyl complex (see the ESI† for details). The internal alkynes 3-hexyn-2-ol and 1,3-diphenyl-2-propyn-1-ol were used in an attempt to obtain the oxetene intermediate in an NMR tube. Unfortunately, we were not able to obtain the oxetene intermediate (see the ESI†) although we changed the temperature (up to −50 °C), the base (bis(dimethylamino)naphthalene and potassium carbonate), the solvent ($CDCl_3$ and CD_3OD) and the gold complex (**1**-OTf and **1**-TFA). Failure to isolate the oxetene intermediate is, however, still consistent with the computationally proposed mechanism, since this species is predicted to very easily undergo electrocyclic ring opening (the conversion from the INT to PC requires an activation barrier of 4.5 kcal mol^{-1}; see Fig. 2).

With the aim of further understanding the experimental conditions which may affect the mechanism, in Fig. 4 we compare the gas-phase profile for the OTf$^-$-assisted nucleophilic attack with those accounting for (i) the use of more polar solvents and (ii) the presence of traces of acid.

Possible traces of acid in solution are accounted for protonating the OTf$^-$ anion. As shown in Fig. 4, with the HOTf species assisting the attack, no intermediate is formed since HOTf cannot behave as a proton-shuttle. As a result, the reaction proceeds *via* TS_{acid} to PC_{acid}, with the latter being thermodynamically less stable with respect to the OTf$^-$ assisted attack (−6.2 *vs.* −19.9 kcal mol^{-1}, respectively) and with a slightly higher activation barrier (37.7 kcal mol^{-1}), consistent with the experimental findings. This result shows that for the formation of the oxetene intermediate to occur, the anion hydrogen bond-acceptor ability is essential. As previously pointed out, the role of the anion in gold-catalyzed processes can be highly modified by the polarity of the solvent.[9] In the case of low-polarity *p*-cymene, the presence of a catalytically active ion pair is reasonable (*i.e.*, [NHC-Au(I)-(1-phenyl-2-propyn-1-ol)]$^+$X$^-$), with the counterion playing an active role in the reaction. By increasing the polarity of the solvent, we expect that the active free ions are the predominant species in solution (*i.e.*, [NHC-Au(I)-(1-phenyl-2-propyn-1-ol)]$^+$ + X$^-$), with the counterion losing its fundamental role. As shown in Fig. 4, when the anion is replaced with an explicit molecule of a neoteric polar solvent (*i.e.*, GVL), a reactivity change is observed. The structure of TS_{GVL} suggests that GVL is not able to substitute the role of OTf$^-$ in accepting the proton from the substrate hydroxyl group, resulting in a one-step intramolecular nucleophilic attack without the formation of the intermediate and in a slightly higher activation energy barrier (33.4 kcal mol^{-1}).

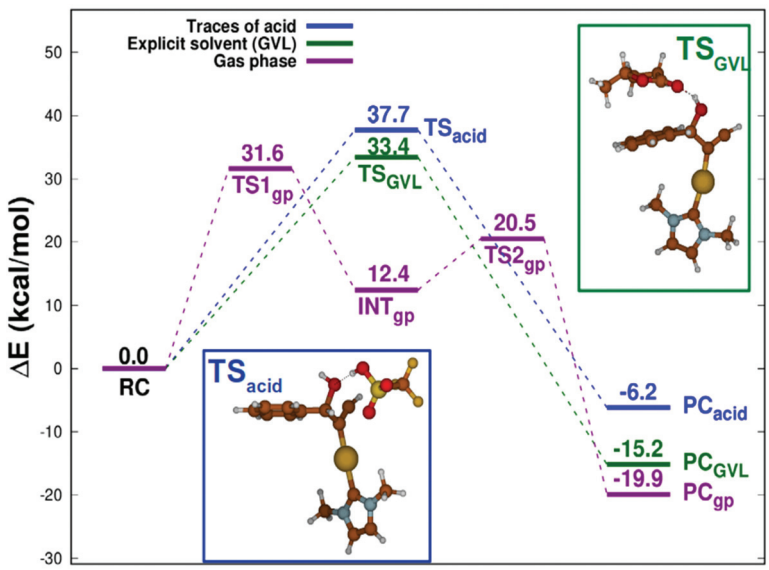

Fig. 4 Energy profiles (BP86/ZORA/D3//B2PLYP) of the intramolecular nucleophilic attack of 1-phenyl-2-propyn-1-ol catalyzed by the [Au(I)-NHC′]$^+$ complex under three different conditions: gas phase (OTf$^-$) (the violet line), in the presence of explicit traces of acid (HOTf) (the blue line) and with an explicit molecule of the polar solvent (γ-valerolactone) replacing the anion (the green line). The structures of the transition states are shown for the acid (TS_{acid}) and polar solvent (TS_{GVL}) conditions. Energy values refer to the corresponding reactant complex RC taken as zero.

Conclusions

In conclusion, we propose here a commonly accepted mechanism for gold(I)-catalyzed alkyne reactions which can also explain the gold-catalyzed Meyer–Schuster rearrangement of 1-phenyl-2-propyn-1-ol in *p*-cymene showing that it accounts for the formation of an unprecedented gold-oxetene intermediate *via* 4-*endo-dig* cyclization. This mechanism well rationalizes the experimental reactivity which is highly dependent on both anion and solvent effects. Our theoretical calculations give insights into the experimental conditions that may modify the mechanism, such as the presence of acid traces and the nature of the solvent. This study further consolidates the use of green solvents instead of traditional VOS in gold catalysis.[9]

Conflicts of interest

There are no conflicts to declare.

Acknowledgements

D. S., L. B. and P. B. are grateful to the MIUR and the University of Perugia (AMIS, "Dipartimenti di Eccellenza 2018–2022" program and "Fondo Ricerca di Base 2019").

References

1 B. Zhang and T. Wang, *Asian J. Org. Chem.*, 2018, **7**, 1758–1783.
2 (*a*) K. H. Meyer and K. Schuster, *Ber. Dtsch. Chem. Ges.*, 1922, **55**, 819–823; (*b*) S. Swaminathan and K. V. Narayanan, *Chem. Rev.*, 1971, **71**, 429–438.
3 (*a*) M. Georgy, V. Boucard and J. M. Campagne, *J. Am. Chem. Soc.*, 2005, **127**, 14180–14181; (*b*) S. S. Lopez, D. A. Engel and G. B. Dudley, *Synlett*, 2007, 949–953; (*c*) I. L. Sang, Y. B. Ji, H. S. So and K. C. Young, *Synthesis*, 2007, 2107–2114; (*d*) D. A. Engel, S. S. Lopez and G. B. Dudley, *Tetrahedron*, 2008, **64**, 6988–6996.
4 N. Marion, P. Carlqvist, R. Gealageas, P. De Frémont, F. Maseras and S. P. Nolan, *Chem. – Eur. J.*, 2007, **13**, 6437–6451.
5 (*a*) D. Zuccaccia, L. Belpassi, A. Macchioni and F. Tarantelli, *Eur. J. Inorg. Chem.*, 2013, 4121–4135; (*b*) D. Zuccaccia, A. Del Zotto and W. Baratta, *Coord. Chem. Rev.*, 2019, **396**, 103–116; (*c*) M. Jia and M. Bandini, *ACS Catal.*, 2015, **5**, 1638–1652.
6 (*a*) L. Biasiolo, M. Trinchillo, P. Belanzoni, L. Belpassi, V. Busico, G. Ciancaleoni, A. D'Amora, A. Macchioni, F. Tarantelli and D. Zuccaccia, *Chem. – Eur. J.*, 2014, **20**, 14594–14598; (*b*) M. Gatto, A. Del Zotto, J. Segato and D. Zuccaccia, *Organometallics*, 2018, **37**, 4685–4691; (*c*) M. Gatto, P. Belanzoni, L. Belpassi, L. Biasiolo, A. Del Zotto, F. Tarantelli and D. Zuccaccia, *ACS Catal.*, 2016, **6**, 7363–7376.
7 G. Ciancaleoni, L. Belpassi, D. Zuccaccia, F. Tarantelli and P. Belanzoni, *ACS Catal.*, 2015, **5**, 803–814.
8 (*a*) J. Schießl, J. Schulmeister, A. Doppiu, E. Wörner, M. Rudolph, R. Karch and A. S. K. Hashmi, *Adv. Synth. Catal.*, 2018, **360**, 2493–2502; (*b*) J. Schießl, J. Schulmeister, A. Doppiu, E. Wörner, M. Rudolph, R. Karch and A. S. K. Hashmi, *Adv. Synth. Catal.*, 2018, **360**, 3949–3959; (*c*) Z. Lu, T. Li, S. R. Mudshinge, B. Xu and G. B. Hammond, *Chem. Rev.*, 2021, DOI: 10.1021/acs.chemrev.0c00713.
9 M. Gatto, W. Baratta, P. Belanzoni, L. Belpassi, A. Del Zotto, F. Tarantelli and D. Zuccaccia, *Green Chem.*, 2018, **20**, 2125–2134 and reference therein.
10 A. Zhdanko and M. E. Maier, *ACS Catal.*, 2015, **5**, 5994–6004.
11 M. Gatto, A. Del Zotto, J. Segato and D. Zuccaccia, *Organometallics*, 2018, **37**, 4685–4691.
12 (*a*) A. Stephen and A. S. K. Hashmi, *Angew. Chem., Int. Ed.*, 2010, **49**, 5232–5241; (*b*) T. Lauterbach, A. M. Asiri and A. S. K. Hashmi, *Adv. Organomet. Chem.*, 2014, **62**, 261–297.
13 (*a*) C. Riplinger, B. Sandhoefer, A. Hansen and F. Neese, *J. Chem. Phys.*, 2013, **139**, 134101; (*b*) C. Riplinger and F. Neese, *J. Chem. Phys.*, 2013, **138**, 34106.
14 G. Ciancaleoni, S. Rampino, D. Zuccaccia, F. Tarantelli, P. Belanzoni and L. Belpassi, *J. Chem. Theory Comput.*, 2014, **10**, 1021–1034.
15 (*a*) G. Bistoni, P. Belanzoni, L. Belpassi and F. Tarantelli, *J. Phys. Chem. A*, 2016, **120**, 5239–5247; (*b*) L. D'Amore, G. Ciancaleoni, L. Belpassi, F. Tarantelli, D. Zuccaccia and P. Belanzoni, *Organometallics*, 2017, **36**, 2364–2376.
16 (*a*) I. V. Alabugin, K. Gilmore and M. Manoharan, *J. Am. Chem. Soc.*, 2011, **133**, 12608–12623; (*b*) R. Dorel and A. M. Echavarren, *Chem. Rev.*, 2015, **115**, 9028–9072.
17 (*a*) B. Alcaide, P. Almendros, T. M. Del Campo and I. Fernández, *Chem. Commun.*, 2011, **47**, 9054–9056; (*b*) J. Renault, Z. Qian, P. Uriac and N. Gouault, *Tetrahedron Lett.*, 2011, **52**, 2476–2479; (*c*) R. K. Shiroodi, M. Soltani and V. Gevorgyan, *J. Am. Chem. Soc.*, 2014, **136**, 9882–9885; (*d*) Y. Badrieh, A. Kayyal and J. Blum, *J. Mol. Catal.*, 1992, **75**, 161.